MIXED-DOMAIN MULTI-SIMULATOR STATISTICAL DEVICE MODELING AND YIELD-DRIVEN DESIGN

J.W. Bandler, R.M. Biernacki and S.H. Chen

OSA-97-GA-11-R

July 11, 1997

Proc. 1997 Gallium Arsenide Applications Symposium, Bologna, Italy, September, 1997

MIXED-DOMAIN MULTI-SIMULATOR STATISTICAL DEVICE MODELING AND YIELD-DRIVEN DESIGN

Invited Paper

J.W. Bandler, R.M. Biernacki and S.H. Chen

Optimization Systems Associates Inc.
P.O. Box 8083, Dundas, Ontario, Canada L9H 5E7
osa@osacad.com

Abstract

We present mixed-domain, multi-simulator approaches to device modeling and yield-driven optimization. Intelligent computational interfaces combine and enhance the features of otherwise disjoint simulators. Time-domain, frequency-domain and electromagnetic simulations are integrated for efficient statistical modeling and design with mixed-domain specifications. Our approach is demonstrated by statistical modeling of GaAs MESFETs and yield optimization using, simultaneously, SPICE device models, Sonnet's electromagnetic simulator *em* and OSA's design optimization system OSA90/hope. Space Mapping optimization aligns mode-matching and finite element based electromagnetic simulations.

Introduction

Statistical modeling and design which take into account the manufacturing tolerances and model uncertainties are indispensable for today's microwave CAD, especially for MMIC design (e.g., [1-5]).

Microwave circuit designers are frequently forced to use different CAD systems to address different aspects of their designs [6]. However, incompatible user interfaces and data formats make such a design process tedious and time consuming. For example, the public domain SPICE does not provide means for optimization. Incorporating the results of electromagnetic (EM) simulations of passive subcircuits into SPICE requires an equivalent circuit representation and is not available in an automated fashion. The rigid structure of commercial versions of SPICE permits only limited optimization.

The authors are also with the Simulation Optimization Systems Research Laboratory and the Department of Electrical and Computer Engineering, McMaster University, Hamilton, Ontario, Canada L8S 4L7; http://soya.sos.mcmaster.ca

Intelligent computational interfaces are needed. In this paper we present a flexible approach to mixed-domain, multi-simulator statistical modeling and design. An open architecture interface is used to connect various CAD systems in a uniform and user-friendly manner.

We integrate time-domain, frequency-domain and EM simulations into a versatile optimization environment. We demonstrate multi-simulator applications using SPICE [7], *em* [8], HFSS [9,10], RWGMM [11], all interfaced to OSA90/hope [12] through Empipe [12], Empipe3D [12], Spicepipe [13,14], or a generic Datapipe [12,15].

The mixed-domain multi-simulator approach is demonstrated by several examples. A low-pass filter design including specifications defined in both the time and frequency domains and an amplifier design utilize our interface between SPICE and OSA90/hope. The interface is also used for device modeling. In the design of a small-signal broadband amplifier with microstrip components the MESFET is simulated by SPICE and the microstrip components are analyzed by *em*. Further advantages of the multi-simulator approach are exemplified by Space Mapping [16] optimization with two different EM simulators.

Datapipe Technique for Optimization Interface

Our optimization interface is based on the Datapipe technique. It utilizes interprocess pipe communication to establish high speed data connections between different processes. A schematic of the Datapipe interface between a parent process and a number of child processes is shown in Fig. 1.

The parent communicates with each child through a Datapipe protocol at the parent side and a Datapipe server at the child side. The Datapipe protocol consisting of a set of communication

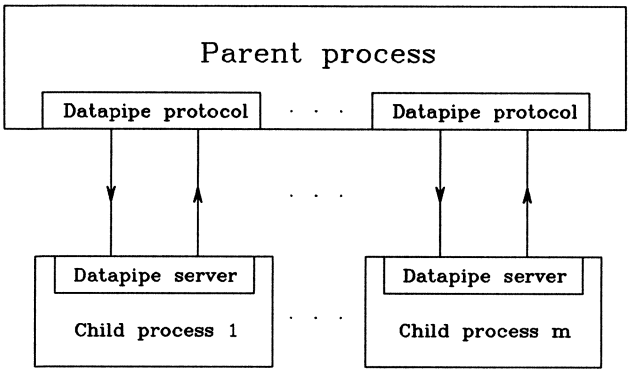

Fig. 1. Datapipe schematic.

standards defines the sequence and meaning of the data fields to be exchanged between the parent and the child. The Datapipe server is a set of functions to be included in the child for reading data from and writing data to the parent. The parent and the child can be totally independent. This is especially suitable for sensitive software since the source code does not need to be revealed.

In general, there is no limit to the number of children that can be interconnected with a single parent through Datapipes. Furthermore, the parent and the children can run on different computers connected through a network. This facilitates distributed computation which can significantly speed up CPU intensive optimization [17].

The Datapipe interfaces between OSA90/hope and several external simulators, including SPICE, AWE [18], TLM [19], *em*, HFSS, and RWGMM, are depicted in Fig. 2.

Mixed-Domain Multi-Simulator Yield-Driven Design: Theory

We consider a parent system and m child systems interfaced through Datapipes as shown in Fig. 1. The parent integrates the simulation results returned from each child and performs the circuit-level simulation and optimization.

Assuming that n_o outcomes are used in yield optimization, responses of the ith outcome $\boldsymbol{\phi}^i$ can be written as

$$\boldsymbol{R}_P(\boldsymbol{\phi}^i) = \boldsymbol{R}_P(\boldsymbol{\phi}^i, \boldsymbol{R}_{C_1}(\boldsymbol{\phi}^i), \boldsymbol{R}_{C_2}(\boldsymbol{\phi}^i), ..., \boldsymbol{R}_{C_m}(\boldsymbol{\phi}^i)) \quad (1)$$

where $i = 1, 2, ..., n_o$, $\boldsymbol{R}_P$ represents the circuit-level responses simulated by the parent and $\boldsymbol{R}_{C_k}$, $k = 1, 2, ..., m$, represents the responses of the subcircuits simulated by the kth child.

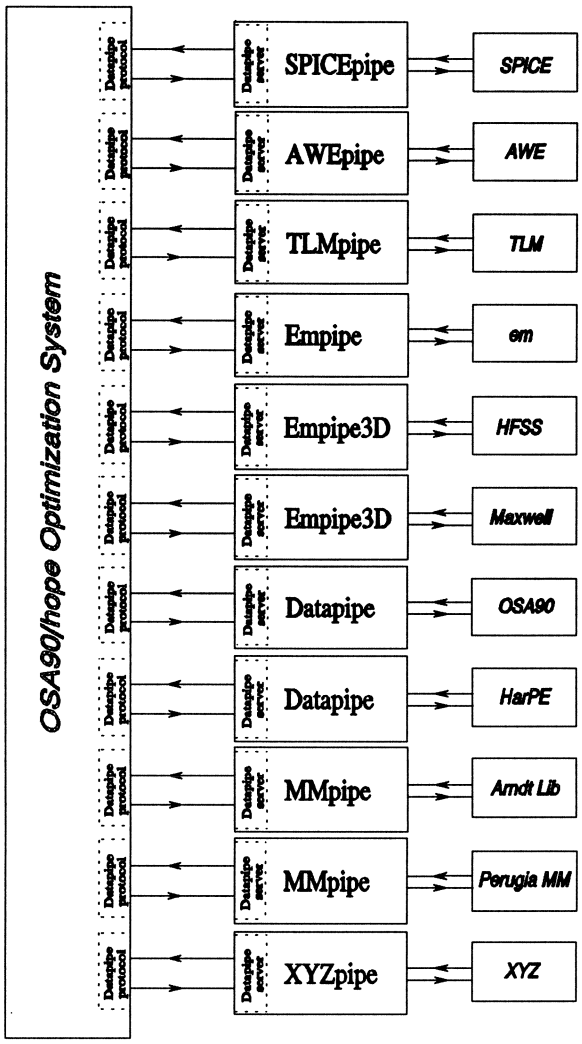

Fig. 2. Datapipe interfaces between OSA90/hope and several external simulators.

Although each child is usually designated to one particular type of simulation, $\boldsymbol{R}_{C_k}$ can be generally expressed as

$$\boldsymbol{R}_{C_k}(\boldsymbol{\phi}^i) = \boldsymbol{R}_{C_k}(\boldsymbol{R}^t_{C_k}(\boldsymbol{\phi}^i), \boldsymbol{R}^f_{C_k}(\boldsymbol{\phi}^i), \boldsymbol{R}^e_{C_k}(\boldsymbol{\phi}^i)) \quad (2)$$

where $\boldsymbol{R}^t_{C_k}$, $\boldsymbol{R}^f_{C_k}$ and $\boldsymbol{R}^e_{C_k}$ represent time-domain responses, frequency-domain responses and EM responses, respectively.

For the ith outcome and the jth specification S_j, $j = 1, 2, ..., n_s$, the error function is defined as

$$e_j(\boldsymbol{\phi}^i) = R_{P_j}(\boldsymbol{\phi}^i) - S_j \quad (3)$$

if S_j is an upper specification, or as

$$e_j(\boldsymbol{\phi}^i) = S_j - R_{P_j}(\boldsymbol{\phi}^i) \quad (4)$$

if S_j is a lower specification.

If all $e_j(\phi^i)$, $j = 1, 2, ..., n_s$, are nonpositive the outcome ϕ^i is acceptable. The design yield is estimated by the ratio of acceptable outcomes (which satisfy all design specifications) to the total number of outcomes considered.

The yield-driven design problem is formulated as

$$\underset{\phi^0}{\text{minimize}} \quad U(\phi^0) = \sum_{i=1}^{n_o} H[\alpha_i v(\phi^i)] \qquad (5)$$

where α_i are positive multipliers and $v(\phi^i)$ is the generalized ℓ_p function as defined in [20]. H can be the one-sided ℓ_1 function [20] or the one-sided Huber function [21].

Mixed-Domain Multi-Simulator Yield-Driven Design: Example

To illustrate the flexibility of mixed-domain multi-simulator yield optimization we consider a simple low-pass filter shown in Fig. 3.

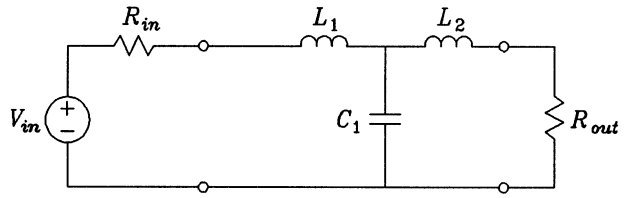

Fig. 3. A simple low-pass LC filter.

The low-pass filter is designed to meet the specifications defined in both the frequency and the time domains. The design procedure consists of nominal design followed by yield optimization.

The specifications are

$$\text{INSL} \le 1.5 \text{ dB} \qquad \text{for } 0 < \omega < 1$$
$$\text{INSL} \ge 25 \text{ dB} \qquad \text{for } \omega > 2.5$$

in the frequency domain, and

$$0.45 \text{ V} \le V_{out} \le 0.55 \text{ V} \qquad \text{for } 3.5 \text{ s} < t < 20 \text{ s}$$

in the time domain, where INSL is the insertion loss, ω the angular frequency in rad/s, t the time and V_{out} the output voltage.

The time-domain simulation is performed by SPICE. The frequency-domain simulation and the mixed-domain optimization are performed by OSA90/hope. L_1, L_2 and C_1 with a uniform distribution within a 10% tolerance are selected as design variables. The yield is increased from 29% at the nominal design to 67% after optimization. Monte Carlo sweeps of the time- and frequency-domain responses are plotted in Fig. 4.

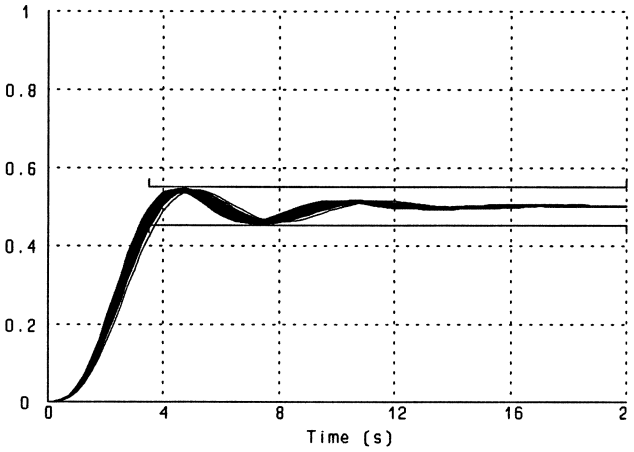

(a)

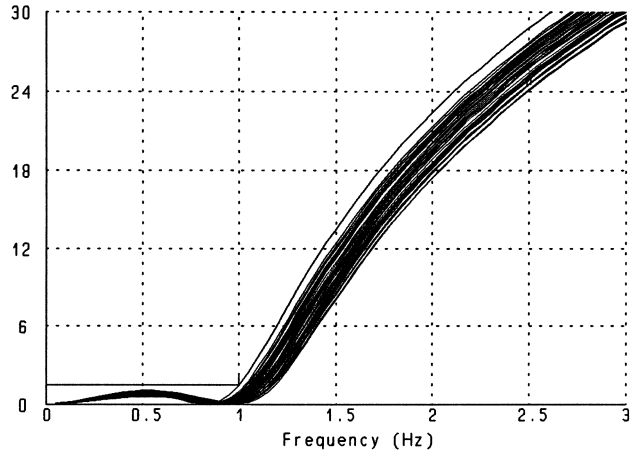

(b)

Fig. 4. Monte Carlo sweeps of the low-pass filter responses in (a) the time domain and (b) the frequency domain.

Integrating SPICE Device Simulation into Circuit Level Optimization

Capturing SPICE Device Models

For the particular application of capturing SPICE device models, SPICE is invoked to simulate the device only. If there is a number of devices in the circuit, all to be simulated by SPICE, the overall circuit responses need to accommodate the individual device responses returned by SPICE.

The SPICE output returned to OSA90/hope may need to be postprocessed. For example, in order to obtain the S parameters of a device we invoke SPICE evaluation of node voltages. In fact, two SPICE simulations are carried out to determine the parameters of a 2-port network. Those node voltages are then converted to the S parameters by using mathematical expressions formulated in the OSA90/hope input file.

Statistical Device Modeling with SPICE and OSA90/hope [22]

Suppose there are n_d sets of data measured from n_d devices and n_i measured responses in the ith data set

$$S^i = [S_1^i \; S_2^i \; ... \; S_{n_i}^i]^T, \quad i = 1, 2, ..., n_d \qquad (6)$$

Corresponding to S^i we have the SPICE responses

$$R_{SP}(\phi^i) = [R_{SP_1}(\phi^i) \; R_{SP_2}(\phi^i) \; ... \; R_{SP_{n_i}}(\phi^i)]^T \qquad (7)$$

where ϕ^i is the ith set of model parameters to be extracted.

For each data set, the error vector is defined as

$$e_{OS}(\phi^i) = [e_{OS_1}(\phi^i) \; e_{OS_2}(\phi^i) \; ... \; e_{OS_{n_i}}(\phi^i)]^T \qquad (8)$$

where individual errors represent the equality constraints of the matching problem

$$e_{OS_j}(\phi^i) = R_{SP_j}(\phi^i) - S_j^i \qquad (9)$$

The subscript *OS* signifies the concept of the optimization space, also used in Space Mapping optimization. The parameter extraction problem is defined as

$$\underset{\phi^i}{\text{minimize}} \; U_{OS}(\phi^i) \qquad (10)$$

where U_{OS} is an objective function such as the ℓ_1, ℓ_2 or the Huber norm. The approach based on parameter extraction followed by postprocessing (PEP) [3] is used to derive the statistical model. For each device outcome the parameter extraction is driven by OSA90/hope's optimizer with the SPICE device model captured as described in the previous subsection. Repeated for each data set, this optimization leads to a sample of individually extracted device models. The model statistics including the mean values, standard deviations and the correlation matrix are then produced by postprocessing this sample of models. The entire PEP process can be, alternatively, directed to a child HarPE [12] connected to OSA90/hope using Datapipe as shown in Fig. 2.

Statistical Modeling of a GaAs MESFET

As an example we consider statistical modeling from a sample of GaAs MESFET measurement data which was obtained by aligning the wafer measurements to consistent bias conditions [5]. There are 35 data sets (devices) containing the small-signal S parameters measured at frequencies from 1 to 21 GHz with a 2 GHz step under two bias conditions.

The equivalent circuit shown in Fig. 5 is used to model the GaAs MESFET. There are 18 model parameters. The parameter statistics obtained by PEP include the mean values, standard deviations, discrete density functions (DDF) and correlation matrix. The parameter mean values and standard deviations are listed in Table I.

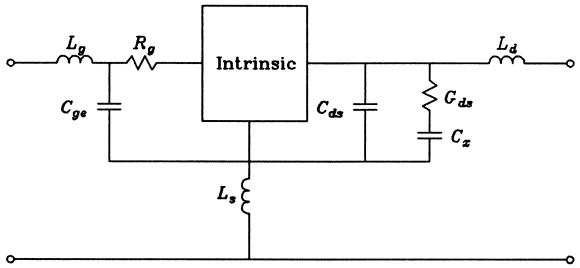

Fig. 5. Equivalent circuit for the SPICE MESFET model.

TABLE I

PARAMETER MEAN VALUES AND STANDARD DEVIATIONS OF THE STATISTICAL SPICE MESFET MODEL

Parameter	Mean	Standard Deviation (%)
C_{gs} (pF)	0.4651	2.87
C_{gd} (pF)	0.0293	2.52
λ (1/V)	4.046×10^{-3}	9.75
V_{to} (V)	-2.4863	5.32
β (A/V^2)	0.0135	5.64
B (1/V)	2.3032×10^{-3}	9.44
α (1/V)	1.9413	7.61
R_d (Ω)	0.0111	8.35
R_s (Ω)	6.5941	5.15
PB (V)	0.6279	7.80
R_g (Ω)	3.7129	6.62
G_{ds} (1/Ω)	3.5593×10^{-3}	2.28
C_{ds} (pF)	0.0485	2.50
L_g (nH)	0.0306	7.97
L_d (nH)	0.0783	9.11
L_s (nH)	0.0344	3.40
C_{ge} (pF)	0.0379	9.96
C_x (pF)	20.0	-

Parameters C_{gs} through PB are the intrinsic SPICE MESFET parameters [6]. Parameters R_g through C_x are the extrinsic parameters with C_x (pF) assumed fixed (non-statistical), see Fig. 5.

To verify the statistical model we compare the statistics of the model responses estimated by Monte Carlo simulation with those of the data.

Table II lists the mean values and standard deviations of S parameters and drain currents from the model and data at two bias points. We can see very good agreement between data and the model responses for the mean values. Some discrepancies in standard deviations are likely due the inadequate statistical modeling capabilities of equivalent circuit models [3].

TABLE II

MEAN VALUES AND STANDARD DEVIATIONS OF DATA AND SPICE MODEL RESPONSES*

Bias 1: $V_G = -0.5$ V, $V_D = 5$ V.

	Data		SPICE MODEL	
	Mean	Dev. (%)	Mean	Dev. (%)
$Re\{S_{11}\}$	-0.197	9.18	-0.192	12.5
$Im\{S_{11}\}$	-0.756	1.1	-0.747	1.07
$Re\{S_{12}\}$	0.0733	2.7	0.0770	3.1
$Im\{S_{12}\}$	0.0519	2.36	0.0527	4.89
$Re\{S_{21}\}$	-0.212	8.35	-0.432	15.2
$Im\{S_{21}\}$	1.78	1.22	1.736	8.71
$Re\{S_{22}\}$	0.440	1.43	0.434	3.33
$Im\{S_{22}\}$	-0.364	0.89	-0.364	0.96
I_d (A)	0.0401	8.16	0.0407	14.7

Bias 2: $V_G = -0.7$ V, $V_D = 5$ V.

	Data		SPICE MODEL	
	Mean	Dev. (%)	Mean	Dev. (%)
$Re\{S_{11}\}$	-0.153	12.1	-0.170	13.7
$Im\{S_{11}\}$	-0.764	1.0	-0.760	1.01
$Re\{S_{12}\}$	0.0770	2.71	0.0784	2.93
$Im\{S_{12}\}$	0.0559	2.46	-0.054	4.68
$Re\{S_{21}\}$	-0.230	6.99	-0.433	15.3
$Im\{S_{21}\}$	1.687	1.67	1.650	9.22
$Re\{S_{22}\}$	0.439	1.44	0.442	3.27
$Im\{S_{22}\}$	-0.367	0.89	-0.366	0.97
I_d (A)	0.0332	9.51	0.0338	16.1

* S parameters at 11 GHz.

Yield-Driven Design of an Amplifier

The circuit schematic of a small-signal amplifier [2] is shown in Fig. 6. The MESFET is simulated in SPICE with the foregoing statistical model. The SPICE results are returned to OSA90/hope through Spicepipe for circuit-level simulation and optimization.

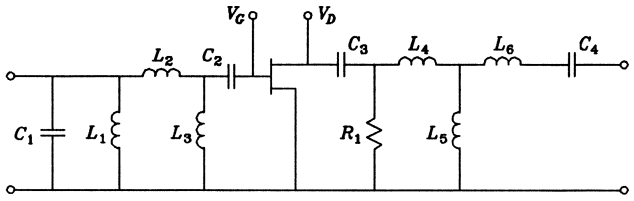

Fig. 6. The small-signal amplifier.

The design specifications are

$$7.25 \text{ dB} < |S_{21}| < 8.75 \text{ dB}$$
$$|S_{11}| < 0.5$$
$$|S_{22}| < 0.5$$

for frequencies from 8 to 12 GHz.

The matching circuit elements, namely, L_1, L_2, L_3, L_4, L_5, L_6, C_1, C_2, C_3, C_4 and R_1, are chosen as design variables with a uniform distribution within a 5% tolerance. A total of 28 statistical parameters is considered. After optimization, the yield is increased from 16% at the nominal design to 52%. The histograms of $|S_{21}|$ at 12 GHz before and after optimization are depicted in Fig. 7.

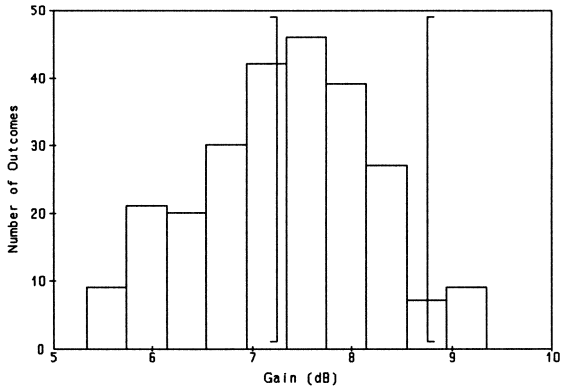

(a)

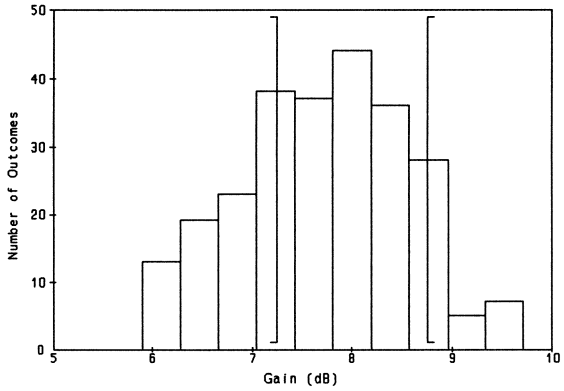

(b)

Fig. 7. Histograms of the gain of the small-signal amplifier at 12 GHz (a) before and (b) after yield optimization.

Combined *em*/SPICE Yield-Driven Design [22]

To illustrate design utilizing simultaneously EM simulations and SPICE device modeling we consider a broadband small-signal amplifier with microstrip components [23] as shown in Fig. 8.

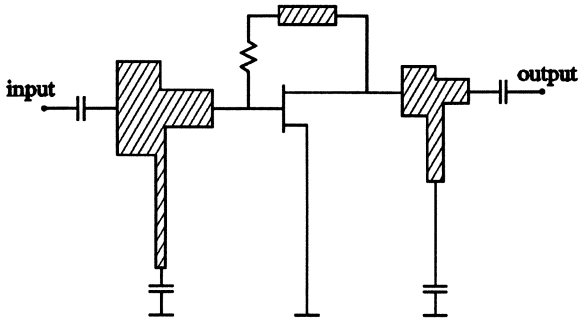

Fig. 8. Broad-band small-signal amplifier with microstrip components.

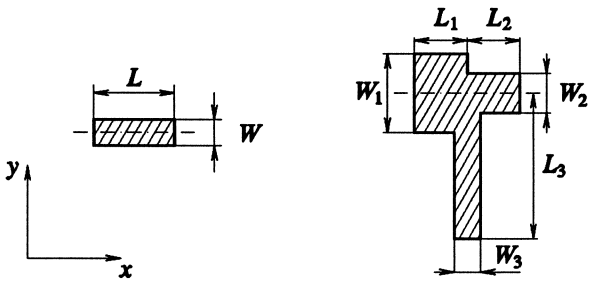

Fig. 9. Parameters of the feedback microstrip line and the microstrip T-structures.

The specification is

$$7 \text{ dB} \le |S_{21}| \le 8 \text{ dB} \quad \text{for} \quad 6 \text{ GHz} \le f \le 18 \text{ GHz}$$

The MESFET is simulated by SPICE using the model shown in Fig. 5. In this case the model parameters and their statistics are different from those listed in Table I. They are obtained by PEP from synthetic data generated by Monte Carlo simulation using the model given in [23].

The passive microstrip components are accurately simulated by *em* utilizing the line and the T-structure primitives of the Empipe [12] library. Each of the microstrip T-structures is defined by six geometrical parameters and the feedback microstrip line is defined by two geometrical parameters, as shown in Fig. 9.

Following [23], we choose W_{g1}, L_{g1}, W_{g2}, L_{g2} of the gate T-structure and W_{d1}, L_{d1}, W_{d2}, L_{d2} of the drain T-structure as design variables. W_{g3}, L_{g3}, W_{d3} and L_{d3} of the T-structures, W and L of the feedback microstrip line, as well as all the MESFET parameters are not optimized. The circuit-level simulation and optimization are carried out by OSA90/hope.

For statistical design we assume a uniform distribution within a 0.5 mil tolerance for all geometrical parameters. Yield at the nominal minimax solution is 43%. It is increased to 74% after yield optimization, which was performed using 50 outcomes. Fig. 10 shows the run charts before and after yield optimization for all of the 250 outcomes used in yield estimation at the frequency of 18 GHz. Clearly, many more outcomes meet the specification on $|S_{21}|$ after yield optimization.

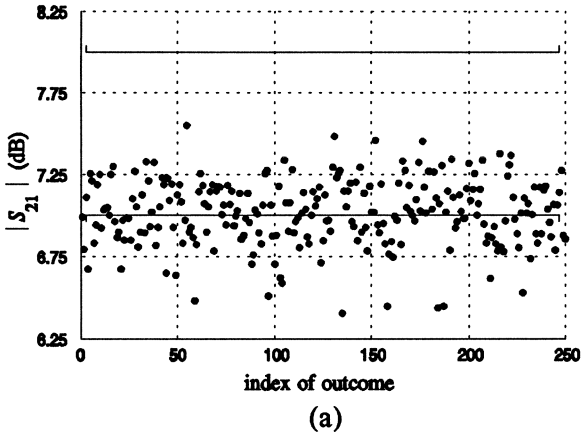

Fig. 10. Run charts of the $|S_{21}|$ response of the broad-band small-signal amplifier at 18 GHz (a) before and (b) after yield optimization. 250 outcomes are used.

Space Mapping Optimization Using MM/Network Theory and FEM [24]

The multi-simulator approach is particularly relevant and suitable for the Space Mapping optimization technique. By definition, the procedure utilizes simultaneously two models of

different accuracy and computational efficiency. Such models would normally be facilitated by two disjoint simulators [16,24-26].

In this Space Mapping optimization example, the mode-matching (MM) waveguide library [11] serves as the OS model, and the finite element (FEM) simulator Maxwell Eminence [10] as the EM model. The flow diagram of the procedure is outlined in Fig. 11. We address the design of the H-plane resonator filter shown in Fig. 12. The waveguide cross-section is 15.8 × 7.9 mm, while the thickness of the irises is t = 0.4 mm. The radius of the corners is R = 1 mm. The iris and resonator dimensions d_1, d_2, l_1 and l_2 are selected as the optimization variables.

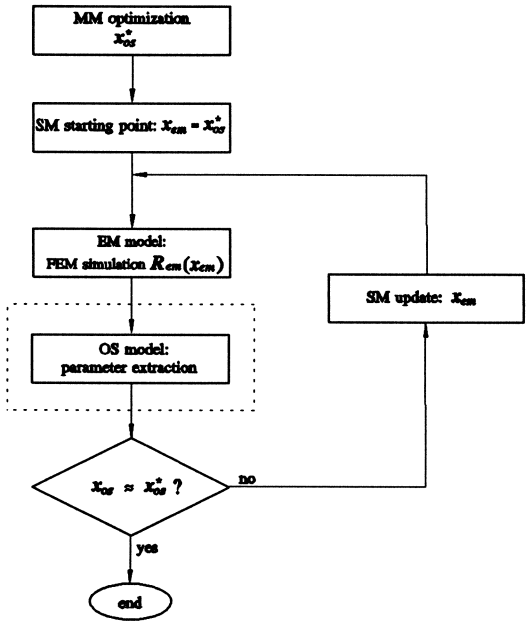

Fig. 11. Flow diagram of the Space Mapping optimization (SM) procedure concurrently exploiting the hybrid MM/network theory and FEM simulation techniques and statistical parameter extraction.

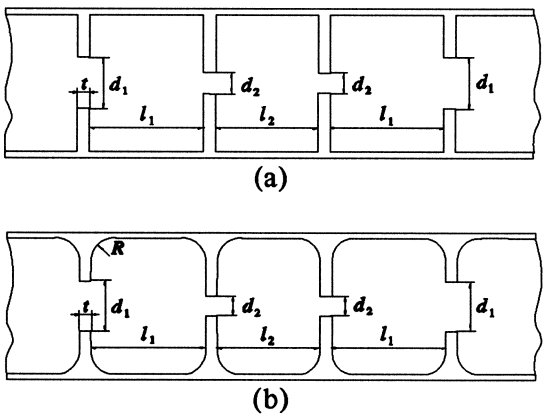

Fig. 12. Structures for Space Mapping optimization: (*a*) OS model, for hybrid MM/network theory; (*b*) fine model, for FEM analysis.

First, minimax optimization of the OS model (Fig. 12(a)) is performed. The following specifications provided by Arndt [27] are used

$$|S_{21}| \text{ (dB)} < -35 \quad \text{for } 13.5 \le f \le 13.6 \text{ GHz}$$
$$|S_{11}| \text{ (dB)} < -20 \quad \text{for } 14.0 \le f \le 14.2 \text{ GHz}$$
$$|S_{21}| \text{ (dB)} < -35 \quad \text{for } 14.6 \le f \le 14.8 \text{ GHz}$$

The minimax solution x_{os}^* is d_1 = 6.04541, d_2 = 3.21811, l_1 = 13.0688 and l_2 = 13.8841. It yields the target response for Space Mapping. Focusing on the passband, we treat responses in the region 13.96 ≤ f ≤ 14.24 GHz. The responses obtained using both models at the point x_{os}^* are shown in Fig. 13. Some discrepancy is evident.

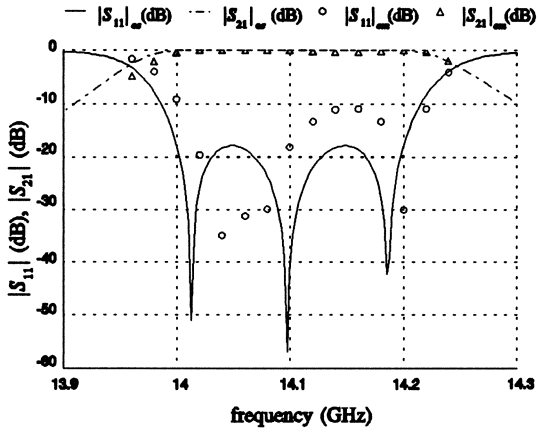

Fig. 13. Magnitudes of S_{11} and S_{21} of the H-plane filter before Space Mapping optimization, as simulated using RWGMM (curves) and Maxwell Eminence (points).

The SM solution shown in Fig. 14 was obtained after only 4 simulations by Maxwell Eminence. Fifteen sample points were used with Maxwell Eminence. This SM solution has been verified by direct optimization of the filter.

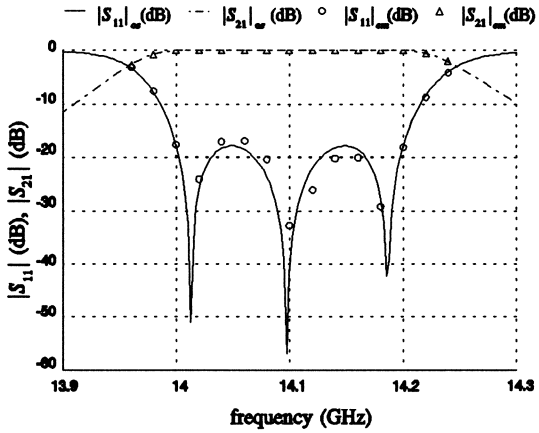

Fig. 14. Space Mapping optimized FEM responses (points) of the H-plane filter compared with the target OS responses (curves).

Conclusions

We have described the Datapipe open architecture technique for interfacing disjoint simulators. Using this technique we have integrated a number of simulators into a powerful optimization environment facilitating mixed-domain nominal and statistical device modeling and circuit design. Our approach has been exemplified by statistical modeling of GaAs MESFETs and yield-driven design of several circuits. Accurate EM field-level simulations have been combined with SPICE device modeling and powerful circuit-level optimization. The multi-simulator approach is particularly relevant to the Space Mapping optimization technique. The advantages of such an approach have been demonstrated using two different EM simulators, namely mode-matching and finite element.

Acknowledgement

This work was supported in part by Optimization Systems Associates Inc. and in part by the Natural Sciences and Engineering Research Council of Canada under Grants OGP0007239, OGP0042444, STR0167080 and through the Micronet Network of Centres of Excellence. The authors would like to thank Sonnet Software, Inc., Ansoft Corp., and Prof. Fritz Arndt of the University of Bremen, Germany, for making their respective software available for this work.

References

[1] J.W. Bandler, R.M. Biernacki, Q. Cai, S.H. Chen, S. Ye and Q.J. Zhang, "Integrated physics-oriented statistical modeling, simulation and optimization," *IEEE Trans. Microwave Theory Tech.*, vol. 40, 1992, pp. 1374-1400.

[2] J.W. Bandler, S. Ye, Q. Cai, R.M. Biernacki and S.H. Chen, "Predictable yield-driven circuit optimization," *IEEE MTT-S Int. Microwave Symp. Dig.* (Albuquerque, NM), 1992, pp. 837-840.

[3] J.W. Bandler, R.M. Biernacki, S.H. Chen, J. Song, S. Ye and Q.J. Zhang, "Statistical modeling of GaAs MESFETs," *IEEE MTT-S Int. Microwave Symp. Dig.* (Boston, MA), 1991, pp. 87-90.

[4] J.W. Bandler, R.M. Biernacki, Q. Cai and S.H. Chen, "A novel approach to statistical modeling using cumulative probability distribution fitting," *IEEE MTT-S Int. Microwave Symp. Dig.* (San Diego, CA), 1994, pp. 385-388.

[5] J.W. Bandler, R.M. Biernacki, Q. Cai and S.H. Chen, "A robust physics-oriented statistical GaAs MESFET model," *Proc. European GaAs Applications Symp.* (Turin, Italy), 1994, pp. 173-176.

[6] M.A. Schamberger and A.K. Sharma, "A generalized electromagnetic optimization procedure for the design of complex interacting structures in hybrid and monolithic microwave integrated circuits," *IEEE MTT-S Int. Microwave Symp. Dig.* (Orlando, FL), 1995, pp. 1191-1194.

[7] T. Quarles, A.R. Newton, D.O. Pederson and A. Sangiovanni-Vincentelli, *SPICE3 Version 3f4 User's Manual.* Department of Electrical Engineering and Computer Sciences, University of California, Berkeley, CA, 1993.

[8] *em*™, Sonnet Software, Inc., 1020 Seventh North Street, Suite 210, Liverpool, NY 13088.

[9] *HP HFSS*™, HP-EEsof, 1400 Fountaingrove Parkway, Santa Rosa, CA 95401.

[10] *Maxwell® Eminence, Ansoft HFSS*™, *MSC/EMAS*™ *MicroWave Lab*, Ansoft Corporation, Four Station Square, Suite 660, Pittsburgh, PA 15219.

[11] T. Sieverding, U. Papziner, T. Wolf and F. Arndt, "New mode-matching building blocks for common circuit CAD programs," *Microwave Journal*, vol. 36, July 1993, pp. 66-79.

[12] *OSA90/hope*™, *Empipe*™, *Empipe3D*™, *HarPE*™, Optimization Systems Associates Inc., P.O. Box 8083, Dundas, Ontario, Canada L9H 5E7.

[13] R.M. Biernacki, J.W. Bandler, S.H. Chen and P.A. Grobelny, "Spicepipe - a case study of flexible circuit optimization," *Proc. European Conf. Circuit Theory and Design* (Davos, Switzerland), 1993, pp. 1323-1328.

[14] *Spicepipe*™, Research Version, Optimization Systems Associates Inc., P.O. Box 8083, Dundas, Ontario, Canada L9H 5E7.

[15] J.W. Bandler, R.M. Biernacki and S.H. Chen, "Design optimization with external simulators," *COMPUMAG 8th Conf. on the Computation of Electromagnetic Fields* (Sorrento, Italy), 1991, pp. 1061-1064.

[16] J.W. Bandler, R.M. Biernacki, S.H. Chen, P.A. Grobelny and R.H. Hemmers, "Space mapping technique for electromagnetic optimization," *IEEE Trans. Microwave Theory Tech.*, vol. 42, 1994, pp. 2536-2544.

[17] J.W. Bandler, R.M. Biernacki, Q. Cai, S.H. Chen and P.A. Grobelny, "Heterogeneous parallel yield-driven electromagnetic CAD," *IEEE MTT-S Int. Microwave Symp. Dig.* (Orlando, FL), 1995, pp. 1085-1088.

[18] R. Griffith, E. Chiprout, Q.J. Zhang and M. Nakhla, "A CAD framework for simulation and optimization of high-speed VLSI interconnections", *IEEE Trans. Circuits and Systems*, vol. 39, 1992, pp. 893-906.

[19] P.P.M. So, W.J.R. Hoefer, J.W. Bandler, R.M. Biernacki and S.H. Chen, "Hybrid frequency/time domain field theory based CAD of microwave circuit," *Proc. 23rd European Microwave Conf.* (Madrid, Spain), 1993, pp. 218-219.

[20] J.W. Bandler and S.H. Chen, "Circuit optimization: the state of the art," *IEEE Trans. Microwave Theory Tech.*, vol. 36, 1988, pp. 424-443.

[21] J.W. Bandler, R.M. Biernacki, S.H. Chen and K. Madsen, "The Huber concept in device modeling, circuit diagnosis and design centering," *Proc. IEEE Int. Symp. Circuits and Systems* (London, England), 1994, vol. 1, pp. 129-132.

[22] J.W. Bandler, R.M. Biernacki, S.H. Chen and P.A. Grobelny, "Optimization technology for nonlinear microwave circuits integrating electromagnetic simulations," *Int. J. Microwave and Millimeter-Wave Computer-Aided Engineering*, vol. 7, 1997, pp. 6-27.

[23] J.W. Bandler, R.M. Biernacki, S.H. Chen, P.A. Grobelny and S. Ye, "Yield-driven electromagnetic optimization via multilevel multidimensional models," *IEEE Trans. Microwave Theory Tech.*, vol. 41, 1993, pp. 2269-2278.

[24] J.W. Bandler, R.M. Biernacki, S.H. Chen and D. Omeragić, "Space mapping optimization of waveguide filters using finite element and mode-matching electromagnetic simulators," *IEEE MTT-S Int. Microwave Symp. Dig.* (Denver, CO), 1997, pp. 635-638.

[25] J.W. Bandler, R.M. Biernacki, S.H. Chen, R.H. Hemmers and K. Madsen, "Electromagnetic optimization exploiting aggressive space mapping," *IEEE Trans. Microwave Theory Tech.*, vol. 43, 1995, pp. 2874-2882.

[26] J.W. Bandler, R.M. Biernacki, S.H. Chen and Y.F. Huang, "Design optimization of interdigital filters using aggressive space mapping and decomposition," *IEEE Trans. Microwave Theory Tech.*, vol. 45, 1997, pp. 761-769.

[27] F. Arndt, Microwave Department, University of Bremen, P.O. Box 330 440, Kufsteiner Str., NW1, D-28334 Bremen, Germany, 1996, *private communications*.